Location and Geometry of Defects in Composite Laminates from Infrared Images

G. Giorleo and C. Meola

(Submitted 15 August 1997; in revised form 6 March 1998)

An infrared scanning system is employed to analyze defective glass-epoxy laminates. Several specimens, manufactured with insertion of pieces of different materials to simulate either delaminations or inclusions are considered, and tests are performed for varying material, shape, depth, and size of inserts. Each specimen is heated by quartz lamps and viewed by an infrared camera, and thermograms are acquired in time sequence in the transient heating phase. Thermograms are quantitatively analyzed in terms of time temperature profiles along lines through the center of defects. The center of a defect is individuated with high certainty; the size instead is measured (from the temperature profile) much well as much as the defect is positioned at small depth and is large. For each test condition, the measured dimension is related to the real one. This ratio, plotted against time, shows an asymptotic distribution and allows for a simple evaluation of defective laminates.

Keywords composite material, defects, infrared thermography, nondestructive tests

1. Introduction

In the last few years, infrared thermography has been widely used in nondestructive controls of materials (Ref 1-5). This interest is justified by the two dimensionality and noncontact character of the technique. Analysis of subsurface features in solid objects, by means of an infrared scanning radiometer, requires heat energy to be transferred to the object in the active mode and mapping of surface temperatures in the transient heating phase. Obviously, for reliable quantitative information about location and extension of flaws in a laminate, specific image treatments are necessary, which involve image-processing methods, filtering, and restoration (Ref 6-9) to enhance the visibility of defects.

In previous works (Ref 4-5), infrared thermography has been employed to visualize defects, artificially created by implants of different materials such as aluminum, cork, and teflon in a glass-epoxy laminate. Images in time sequence were acquired in the transient heating phase. The thermograms were treated with specific software, and data were presented as local temperature distributions taken along the lines that cross the defects. Temperature differences ΔT between undamaged and damaged zones were calculated from the local temperature profiles. It was found that for a certain size and depth of defects, ΔT increases linearly with time for an interval of approximately 30 s, after that the surface temperature moves toward steady-state conditions (uniform temperature distribution). It was found that in the plane (ΔT, t), for a fixed depth, there is a line fitting the ΔT points with the same size (or diameter in the case of defects with circular section). The angular coefficient of each line depends on the thermal properties of the material (conductivity) and on the width and depth of defects.

The aim of the present study is to acquire information about the position and the extension of defected zones in glass-epoxy laminates from thermographic visualizations. The infrared images, already analyzed in the previous works (Ref 4, 5) are considered with particular attention to the local temperature distributions since the extension of local peaks or valleys is proportional to the defect size. The position of defects in a laminate is easily individuated by putting markers over the laminate surface and by knowing exactly the spatial resolution of the employed lens.

G. Giorleo, D.I.M.P., Dipartimento di Ingegneria dei Materiali e della Produzione, Facoltà di Ingegneria-Università degli Studi di Napoli "Federico II" P.le Tecchio, 80-80125 Napoli; and **C. Meola,** D.E.T.E.C. Dipartimento di Energetica Termofluidodinamica Applicata e Condizionamenti Ambientali, Facoltà di Ingegneria-Università degli Studi di Napoli "Federico II" P.le Tecchio, 80-80125 Napoli. Contact e-mail: carmeola@unina.it.

2. Test Specimens

The samples (150 mm by 150 mm) analyzed in the present work are obtained by a staking sequence of glass-epoxy (M10/50%/759-120CM) resine preimpregnated substrates (0.1 mm thick) positioned at 0° and 90° to have a total thickness of 5 mm. To simulate delaminations or nonhomogeneity (defects), pieces of a material, which has thermal properties (in particular, the conductivity coefficient) quite different from the basic material, are inserted in the laminate. In more detail, the final laminate is obtained by superposition of three thinner prepreg laminates. Holes are drilled over one prepreg where pieces of the different material are inserted, so that this prepreg is positioned between the other two prepreg (with a thin layer of resin in both sides) and subjected to curing process. Each prepreg is manufactured with fixed thickness to allow testing defects of different thicknesses and at different depths.

The defects, artificially created in the laminate, are manufactured in two shapes—circular and rectangular—and of thickness, s, equal to 1 mm and 2 mm. A sketch of the generic test specimen with circular defects is shown in Fig. 1. The three

different materials that are considered are aluminum, cork, and teflon. The conductivity coefficient, λ_d, where d is for defect, is 200 W/m·K for aluminum, 0.036 W/m·K for cork, and 0.26 W/m·K for teflon. Relative to the conductivity of the basic material, the fibers are oriented at 0° and 90°. This leads to 2 different values for the conductivity coefficient; along the longitudinal direction of fibers λ_{bL} = 0.65 W/m·K (b for basic material) while in the transversal direction it is λ_{bT} = 0.40 W/m·K. Since the laminate, under test, includes the same number of fibers in the 2 directions the conductivity coefficient, λ_b, can be assumed to be equal to the average between λ_{bL} and λ_{bT}; so λ_b = 0.525 W/m·K. Either for longitudinal or transversal directions, the conductivity coefficient of the basic material differs enough from that of the material of which defects are made. Each sample generally includes 5 defects of different sizes, of ø diam, ranging from 2 up to 8 mm for the circular shape and of a × b from 2 × 14 mm^2 up to 3.4 × 24 mm^2 positioned at the same depth *p*. Some specimens are manufactured with 5 defects of the same size positioned at 5 different depths from 0.1 mm up to 4 mm; of course, in this case, the laminate includes 5 prepreg with a defect in each of them.

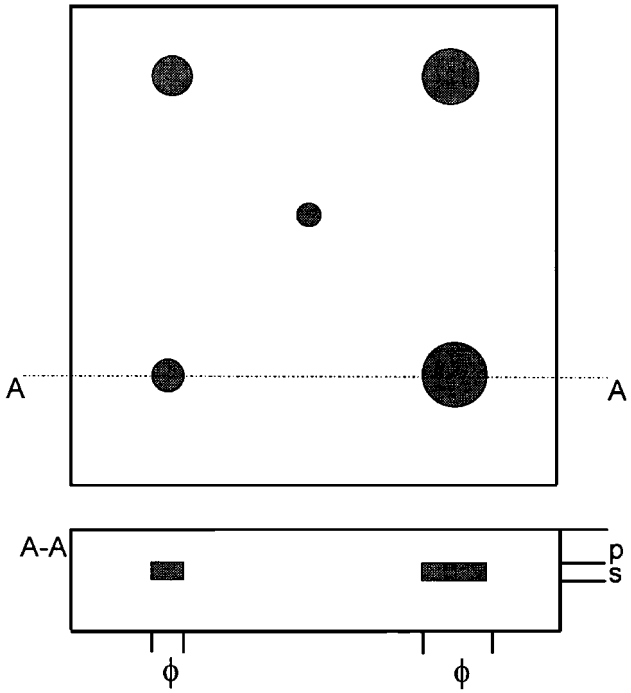

Fig. 1 Sample with defects of circular shape at the same depth

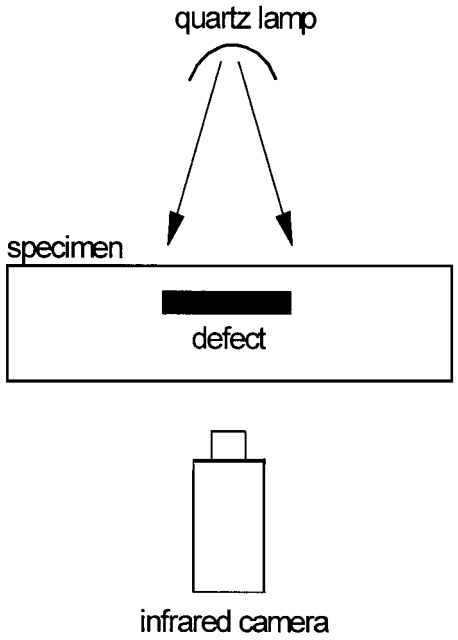

Fig. 2 Test configuration

3. Infrared Thermography and Test Procedure

Heat flows from the hot surface of an object to the cold surface by conduction and needs a certain time (depending on conductivity and thickness of the specific object) to reach steady-state conditions. The presence of a flaw in the subsurface (e.g., a debonding), acts as an obstacle in the heat flow, entailing delay and resulting in cold zones in the surface temperature distribution. If there is inclusion of pieces of a material with a conductivity coefficient higher than that of the basic material, hot zones will be displayed in the surface temperature map. In any case, localized defects in a material give rise to surface temperature differentials and can be detected by thermal methods (Ref 10) provided the depth of the defect is not too large compared to its diameter. The object can also be cooled instead of heated; in this case, a debonding is visualized as a hot zone.

Subsurface flaws are visible in the transient phase of the heating/cooling process, so the timing of the inspection is of utmost importance. Especially when defects of small dimensions and depth are to be detected, instruments that are able to follow the high speed transient phase are recommended. In this context, the infrared thermography is considered a powerful tool.

To allow for thermographic measurements, the specimen surface finish is done with great care; in fact, variations in surface roughness, cleanliness, uniformity of paint, and other surface conditions can entail local variations of the emissivity coefficient and affect the temperature measurement.

The Agema Thermovision 900LW (Agema Infrared Systems, Danderyd, Sweden) is employed. The object radiation is detected by a cryogenically cooled mercury cadmium telluride (MCT) element operating in the 8 to 12 μm band of the infrared spectrum. The good-quality image resolution (230 elements per line at 50% modulation), the sensitivity of 0.08 °C (at ambient temperature), and the high speed acquisition of sequences of images facilitate the detection of transient temperature changes or differentials related to small imperfections in the subsurface of laminates.

As schematically depicted in Fig. 2, the specimen is subjected to heating by quartz lamps (1 K/W); the infrared camera views the rear part (opposite to heating). Sequences of 16 images in 30 s (at intervals of 2 s) are acquired. The anomalies become clearly visible after a certain time interval (depending on

their size and depth), and they appear as cool (black) spots or as hot (white) spots depending on the relative conductivity coefficient between the two materials—that of the laminate and that of the defects.

Additional information about the samples, the experimental apparatus, and the testing procedure was reported by Giorleo and Meola (Ref 4).

4. Shape of Defects

Infrared thermography, due to its two dimensional character, allows defects of whatever shape to be detected; its spatial resolution depends mainly on the camera and the employed optics. The shape of defects can be easily recognized directly from the thermographic images. Generally, the larger the imperfection is and the closer it is to the surface, the greater the temperature differentials are and the more distinguishable is the defect shape. The image relative to circular inserts of teflon of 5 different ϕ diameters—2, 3, 4, 6, and 8 mm—positioned at the same depth of 0.125 mm is shown in Fig. 3. The image relative to defects of rectangular shape 3 mm by 21 mm at 5 different depths of 0.1 mm to 4 mm is instead shown in Fig. 4. The shape of defects is easily identified, and it has to be taken into account that the thermal contrast worsens when the defect is too small or too deep.

5. Dimensions of Defects

The size of defects may be measured directly from the thermograms by knowing the spatial resolution of the employed optics. However, this procedure can be applied successfully only for particular cases (defects of great size and at low depths). Otherwise, the low thermal contrast does not allow for precise measurements. In some cases, specific treatments of images as filtering and restoration may improve defect visualization.

In the present study, the thermograms are analyzed in terms of temperature distributions along lines through the center of defects.

Temperature distributions for defects made of teflon, of 3 mm and 8 mm diameter at several times are shown in Fig. 5. The temperature of the specimen surface initially equal to the ambient temperature after exposure to heating begins to increase and, due to the presence of defects (local differences of conductivity), shows localized differences. In the first time (t = 0 to 2 s), the temperature differences are of the same order of magnitude as the instrument noise, and no measurement is reliable. Later, since the conductivity, λ_d, of the teflon is smaller than that of the basic material, λ_b, local minima appear in the temperature distribution and bring evidence of the presence of

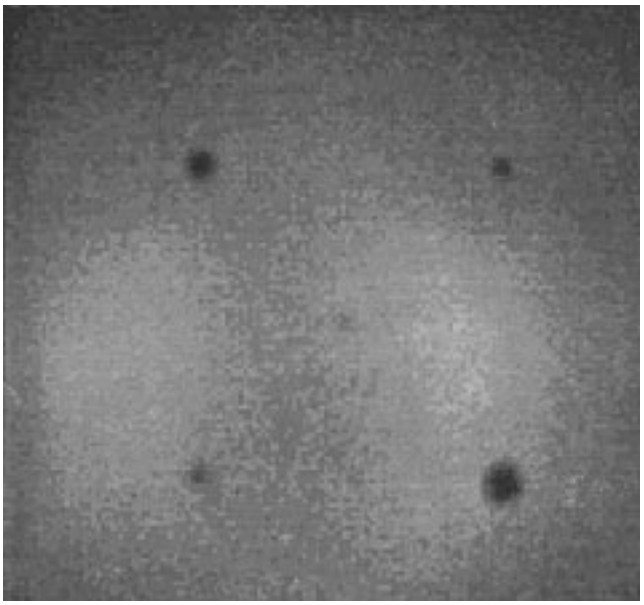

Fig. 3 Thermogram after 16 s to lamp exposure for defects of circular shape positioned at depth p = 0.125 mm

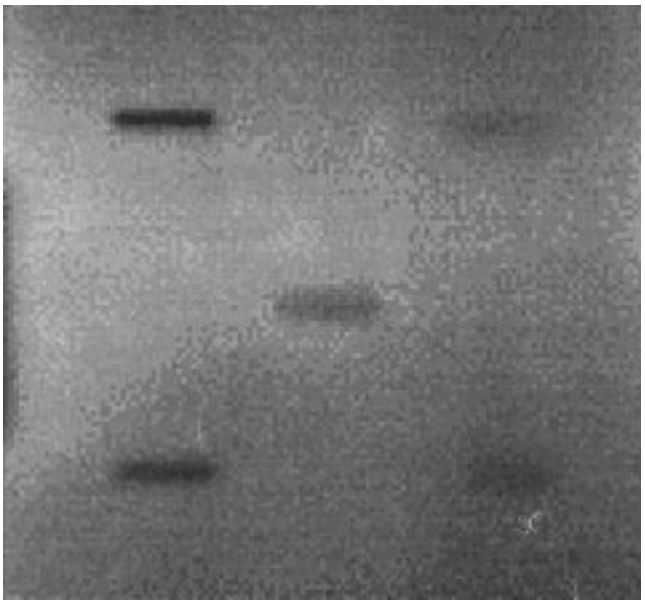

Fig. 4 Thermogram after 16 s to lamp exposure for defects of rectangular shape a = 3 mm, b = 21 mm positioned at different depths from 0.1 mm up to 4 mm

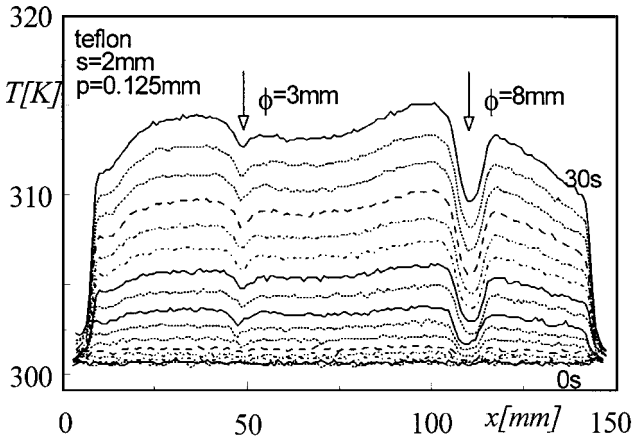

Fig. 5 Temperature distribution for defects of teflon s = 2 mm positioned at p = 0.125 mm

defects; otherwise, in the case of aluminum for which is $\lambda_d < \lambda_b$, the presence of defects, as shown in Fig. 6, is evidenced by local maxima.

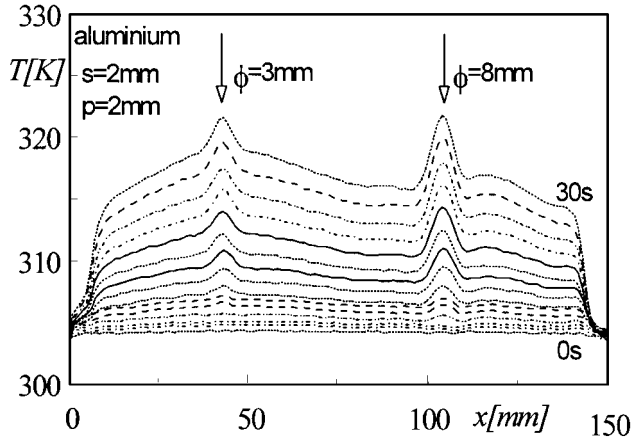

Fig. 6 Temperature distribution for defects of aluminum s = 2 mm positioned at p = 2 mm

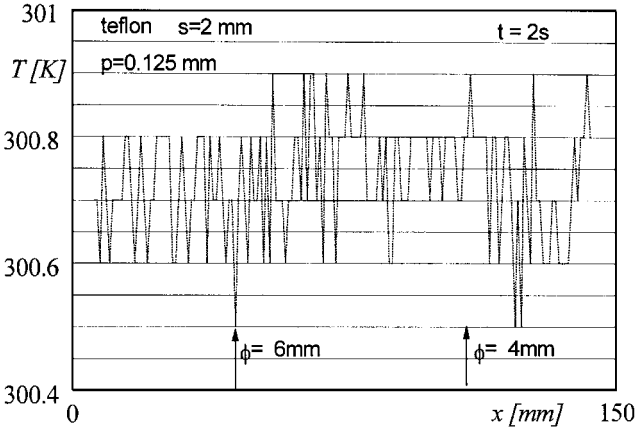

Fig. 7 Temperature distribution after 2 s to heating exposure for defects of teflon s = 2 mm, p = 0.125 mm

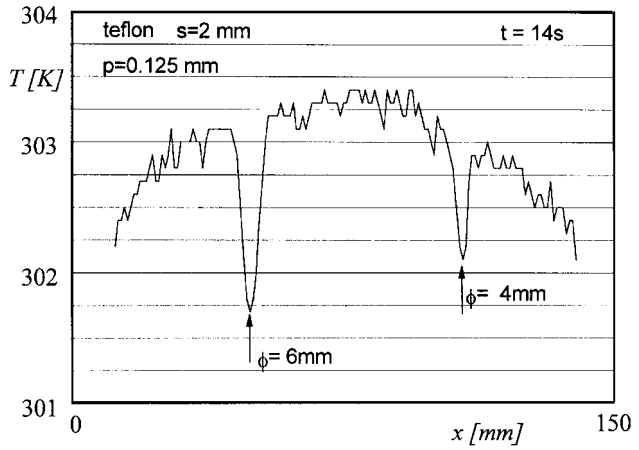

Fig. 9 Temperature distribution after 14 s to heating exposure for defects of teflon s = 2 mm, p = 0.125 mm

As discussed in previous works (Ref 4, 5), the temperature differentials between undamaged and damaged zones, ΔT, vary linearly with time, t; in more detail, each size and/or depth is characterized by a regression line whose slope increases with increasing defect size and with decreasing depth. Information about size and depth of defects may be acquired from the temperature differentials.

Information about location and extension of the defected zone may be simply obtained directly from the temperature distribution against time (like the ones reported in Fig. 5 and 6) by measuring the width of minima (maxima) along the abscissa.

Generally, two problems are encountered when measuring the defect size from temperature distributions. The first problem is linked to the choice of the minimum ΔT value to be considered. The second problem regards the criterion assumed to measure the physical dimension. The minimum ΔT to be associated with the defect detectability has been chosen (Ref 4, 5) to >0.2 K. In fact, from Fig. 7, which refers to the temperature distribution attained by the surface after 2 s to heating exposure, it is evident that the maximum spread about the average value is approximately ±0.15 K (the maximum temperature difference peak-to-peak is 0.3 K).

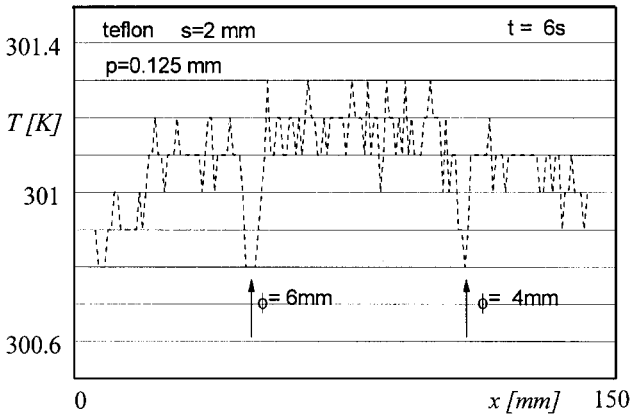

Fig. 8 Temperature distribution after 6 s to heating exposure for defects of teflon of thickness s = 2 mm, depth p = 0.125 mm

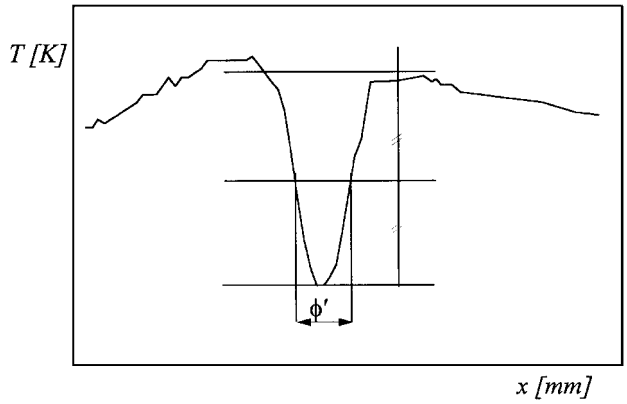

Fig. 10 Conventional measured dimension in a valley relative to a defect made of teflon

As the time to heating exposure increases, the difference between the temperature in the center of the defect and that relative to the basic material becomes more accentuated as shown by comparing Fig. 7, 8, and 9. Defects of smaller size and/or deeper become visible later, but in any case, 30 s may be considered a time interval sufficient for the detectability of defects for all the tested conditions.

The temperature takes its minimum value in the center of the defect and increases slightly going toward the temperature of the undamaged material to have a "V" shape as shown in Fig. 10. The width of such a "V" depends on the size of the defect. However, the problem arises at which height the width has to be taken. The criterion of the middle height of the "V" shape (sketched in Fig. 10) seems to be the most appropriate to minimize the influence of lateral conduction, which involves a decrease in the ΔT value and enlargement of the final part of the "V" shape. By following this method a ϕ' diameter is measured, in the case of circular defects, at the different times (0 to 30 s). The measured ϕ' diameter is related to the real ϕ diameter, and the ratio ϕ'/ϕ is plotted against the time t in Fig. 11 to 17 for different test conditions. For all the tested conditions (variation of size and depth of defects), the experimental points are well fitted by a polynomial law.

Any situation that may lead to errors involving the instrument noise are discarded; no points are taken in the initial heating phase. Notwithstanding the absence of measurement points in the initial times of heating, the correlation curves are forced to start from 0 to reproduce the variation of ϕ' with time. Each curve starts from 0, increases sharply with a certain slope γ, and goes asymptotically toward a limit value Asint. Both γ and Asint depend on the size and depth of defects. In more detail, a surface and width defect, due to the spatial resolution of the infrared scanning system and to the different thermal characteristics of the two materials (basic and defects), is more clearly visible than a smaller subsurface one, and the measured dimension (diameter for circular shape) from the infrared image more closely approaches the real value (Asint = 1). As time increases (that is, after 30 s to heating exposure), the specimen surface goes toward steady-state conditions, the thermal contrast decreases, the defect visibility worsens, and the ϕ'/ϕ curves attain smaller values after the asymptotic one.

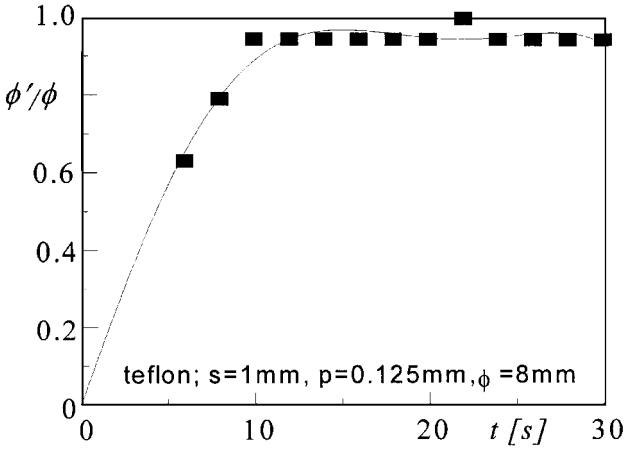

Fig. 11 Distribution of measured to real diameter against time for circular defects of teflon, s = 1 mm, p = 0.125 mm, and ϕ = 8 mm

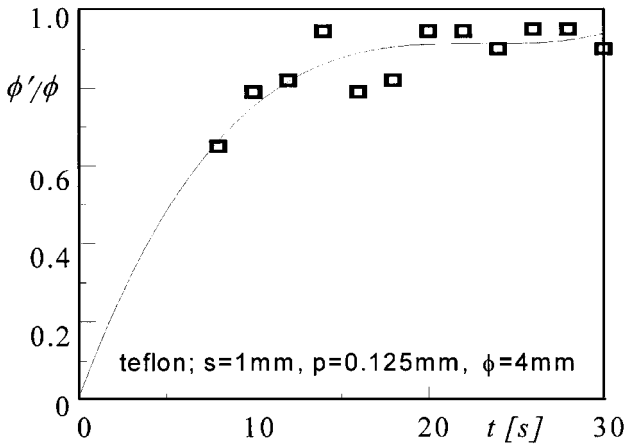

Fig. 12 Distribution of measured to real diameter against time for circular defects of teflon, s = 1 mm, p = 0.125 mm, and ϕ = 4 mm

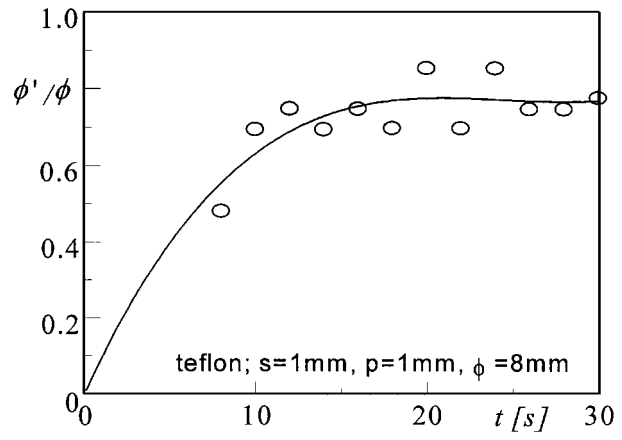

Fig. 13 Distribution of measured to real diameter against time for circular defects of teflon, s = 1 mm, p = 1 mm, and ϕ = 8 mm

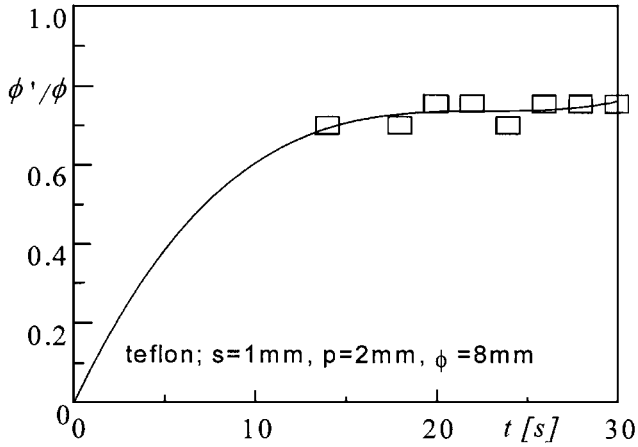

Fig. 14 Distribution of measured to real diameter against time for circular defects of teflon, s = 1 mm, p = 2 mm, and ϕ = 8 mm

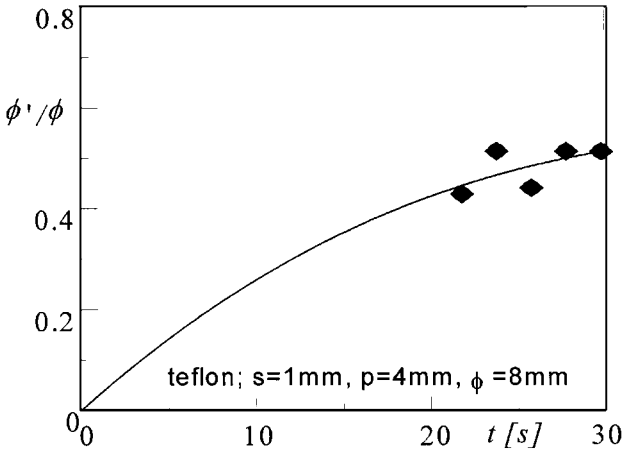

Fig. 15 Distribution of measured to real diameter against time for circular defects of teflon, s = 1 mm, p = 4 mm, and ϕ = 8 mm

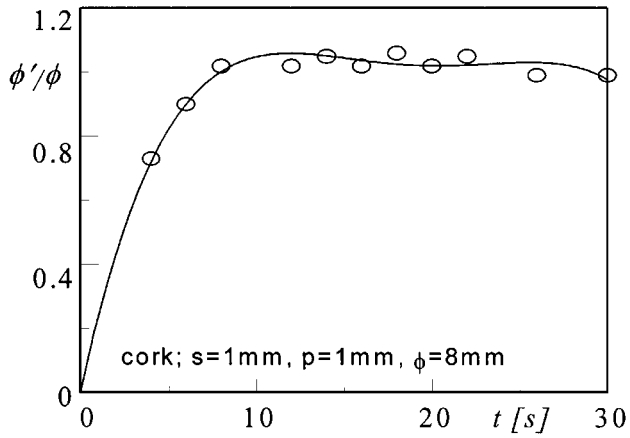

Fig. 16 Distribution of measured to real diameter against time for circular defects of cork, s = 1 mm, p = 1 mm, and ϕ = 8 mm

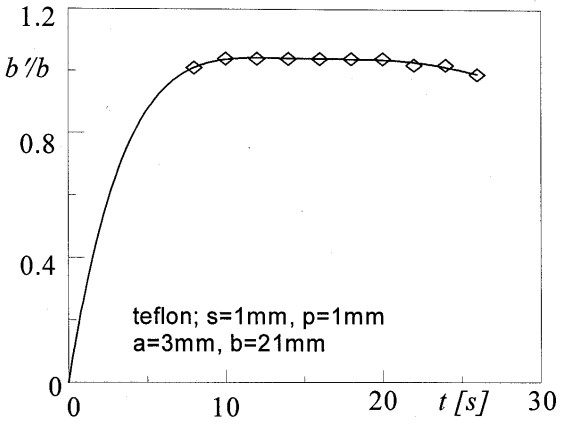

Fig. 17 Distribution of measured to real dimension against time for rectangular defects of teflon, s = 1 mm, p = 1 mm, and b = 21 mm

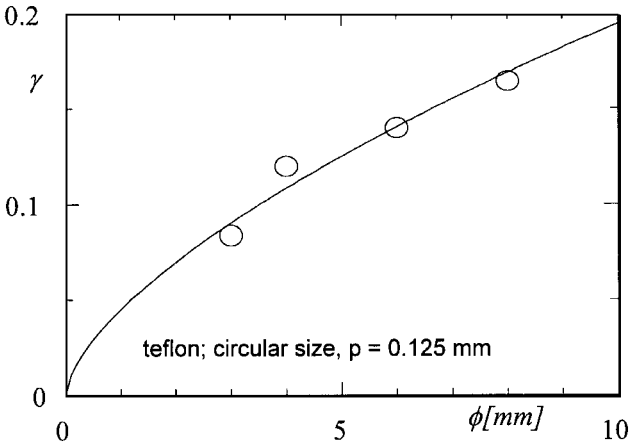

Fig. 18 Distribution of the slope of the correlation curve against the defect diameter for circular defects of teflon, s = 1 mm and p = 0.125 mm

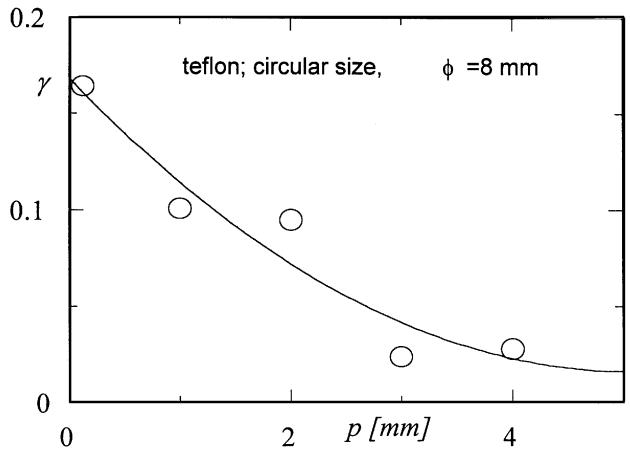

Fig. 19 Distribution of the slope of the correlation curve against the defect depth for circular defects of teflon, s = 1 mm and ϕ = 8 mm

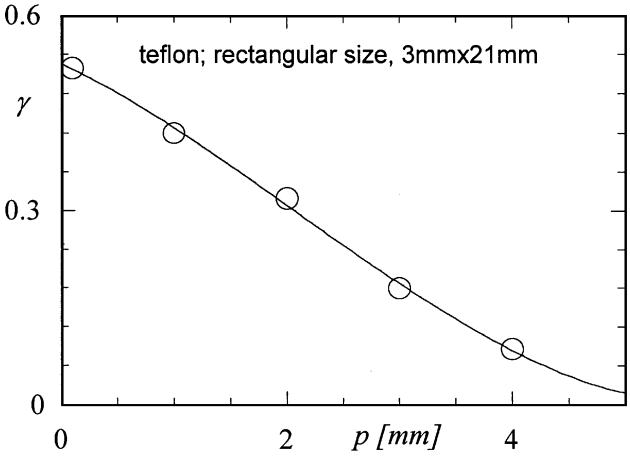

Fig. 20 Distribution of the slope of the correlation curve against the defect depth for rectangular defects of teflon, s = 1 mm, a = 3 mm, and b = 21 mm

To facilitate comparisons, only results relative to defects of thickness s = 1 mm are reported. For defects of teflon of ϕ = 8 mm and p = 0.125 mm (Fig. 11), the Asint value, which approaches unity, is reached after 10 s. As the diameter decreases (for example, ϕ = 4 mm as shown in Fig. 12) or the depth increases (Fig. 13 to 15), a delay is observed in the attainment of the Asint value. In addition, the slope γ of the correlation curve decreases, and Asint assumes values of <1.

In some test conditions, for example, in the case of very low diameters, values of Asint (not shown here) of >1 may be attained. This may be ascribed to lateral conduction effects that entail enlargement of the "V" shape in the final part and can lead to overestimation of the effective dimension.

The behavior of defects is governed by the thermal properties of the material. When inserts are made of cork, whose thermal conductivity is much smaller with respect to glass/epoxy than teflon, the defect visibility is enhanced. In fact, by comparing Fig. 13 and 16, it is evident the higher value of ϕ'/ϕ is attained by defects made of cork. This also leads to higher γ and Asint values. As far as defects with rectangular sections are concerned, the two dimensions a' and b' are measured and related to the corresponding real ones a and b. The ratio b'/b, which refers to defects of teflon for a = 3 mm, b = 21 mm, and p = 1 mm, is reported in Fig. 17. The curve in Fig. 17 is characterized by high values of γ and Asint because the defect is quite large (b = 21 mm).

The γ value represents the slope of the correlation polynomial curve. The asymptotic value Asint is calculated by evaluating, by means of graphical software, the intercept to the ordinate of the line that better fits the points over the plateau of such polynomial curve.

The γ values relative to circular defects are plotted against ϕ in Fig. 18 for p = 0.125 mm and against p in Fig. 19 for ϕ = 8 mm. The γ values relative to rectangular defects are instead plotted against p in Fig. 20. The slope γ might be regarded as a visibility index because it indicates as rapidly as the defect is visualized.

The Asint values are plotted against the defect diameter in Fig. 21 for p = 0.125 mm. As shown, Asint tends to unity as ϕ increases. The variation of Asint with the depth is instead shown in Fig. 22; as p increases, Asint decreases. Both γ and Asint may be considered useful to describe a defective material. For the sake of graphical clearness, all the experimental data are fitted by a simple correlation curve, which is of the power law type for Fig. 18 , 19, 21, and 22 and polynomial for Fig. 20.

6. Location of Defects

The location of defects is easily individuated from the infrared images if the spatial resolution of the employed lens at the tested distance is known. It is well known that minima and/or maxima in the temperature distribution occurs in the defect center. In particular, as shown in Fig. 5 and 6, valleys and peaks are vertically (along the y direction) aligned.

The distance of the lines, intersecting valleys, or peaks from the specimen borders can be assumed as coordinates of defects. The lines intersecting temperature minima for defects of teflon are shown in Fig. 23. In this diagram, the coordinate x can be measured, analogously the coordinate y can be obtained by considering temperature distributions along the vertical direction.

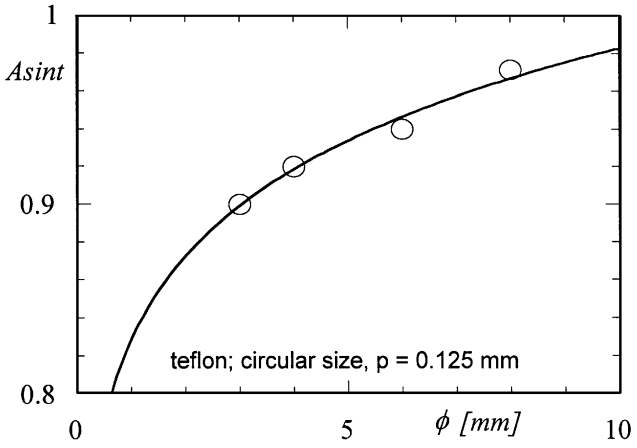

Fig. 21 Distribution of the asymptotic value against the defect diameter for circular defects of teflon, s = 1 mm and p = 0.125 mm

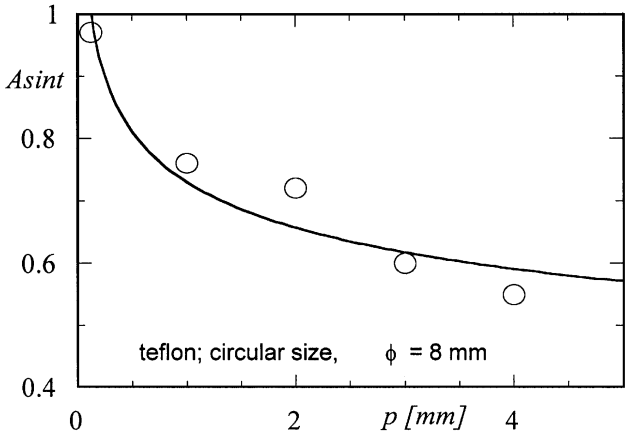

Fig. 22 Distribution of the asymptotic value against the defect depth for circular defects of teflon, s = 1 mm and ϕ = 8 mm

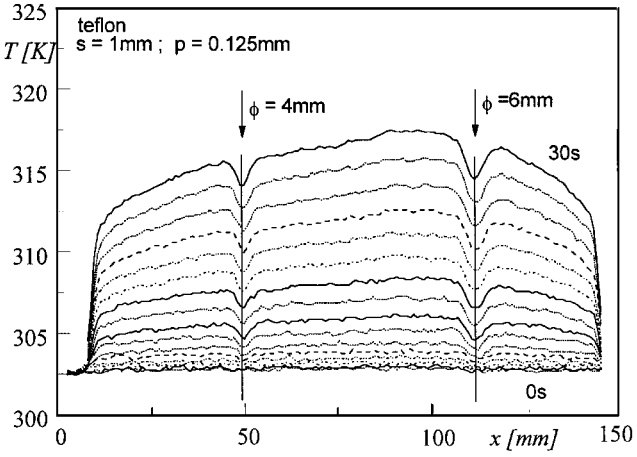

Fig. 23 Location of defects from time temperature distributions

The location of defects can be precisely individuated over a large laminate. In this case, more than one infrared image has to be taken and patched up to reconstruct the entire panel. Each zone is precisely identified by putting markers over the surface and by knowing the viewing distance. Precision depends on correct position of markers.

7. Conclusions

An infrared scanning radiometer has been employed for nondestructive evaluation of industrial materials. Several specimens made of glass epoxy with inserts of aluminum, cork, and teflon have been subjected to thermal excitation and viewed by the infrared camera. Thermograms acquired in time sequence during the transient heating phase give information regarding location and geometry of defects.

Defects can be localized with high precision over a surface of great dimensions and of different shapes by putting markers to individuate the viewed portion and by knowing exactly the spatial resolution of the employed lens. The shape of defects may be directly recognized from the infrared image. The size can be calculated from the temperature distribution along two or more directions by relating to the width of the corresponding valleys or peaks along the different directions. A similar analysis may be applied also in the case of a curved surface by using a proper heating source and by taking into account the directional emissivity decay of the surface itself.

The ratio between measured and real dimension (ϕ'/ϕ or b'/b) starting from 0 (no thermal excitation of the sample) increases sharply with a certain slope γ and goes asymptotically toward a limit value, Asint, in a certain time interval before reaching the steady-state conditions. This asymptotic value, Asint, tends to unity for relatively high values of size and low depth of defects. Both γ and Asint may be assumed as important parameters to characterize the laminate defectivity.

Acquisition of infrared images in 30 s seems sufficient for a clear discernibility of defects made of the different materials, aluminum, cork, and teflon, ranging from 3 up to 81 mm^2 and are positioned at different depths from 0.1 to 4 mm in a glass-epoxy material.

Acknowledgements

The authors wish to express their gratitude to Prof. G. M. Carlomagno (D.E.T.E.C.) for permitting the authors to use the infrared scanning system.

References

1. W.N. Reynolds, Thermographic Methods Applied to Industrial Materials, *Can. J. Phys.*, Vol 64, 1986
2. G. Walle, G. Burgschweiger, and U. Netzelmann, Numerical Modelling of the Defect Response in Pulsed Video Thermography on Samples with Finite Optical Penetration, *QIRT 94, Eurotherm Series 42,* D. Balageas, G. Busse, and G.M. Carlomagno, Ed., EETI Editions, Paris, 1995
3. P. Cielo, X. Maldague, A.A. Déom, and R. Lewak, Thermographic Nondestructive Evaluation of Industrial Materials and Structures, *Mater. Eval.*, The American Society for Nondestructive Testing, Vol 45, 1987
4. G. Giorleo and C. Meola, Nondestructive Evaluation of Defects in Composite Materials by Means of Infrared Thermography, *XXV AIAS National Conf. Int. Conf. on Material Engineering*, (Gallipoli) Le, Vol 1, p 431-438, 1996
5. G. Giorleo and C. Meola, On the Analysis and Modelling of Defects in Composite Laminates, *XXV AIAS National Conf. Int. Conf. on Material Engineering*, (Gallipoli) Le, Vol 1, p 439-446, 1996
6. B. Wiecek and M. Grecki, Advanced Image Processing in Thermography, *QIRT 94, Eurotherm Series 42,* D. Balageas, G. Busse, and G.M. Carlomagno, Ed., EETI Editions, Paris, 1995
7. D. Bougeard, J.P. Vermeulen, and B. Baudoin, Spatial Resolution Enhancement of an IR System by Image Restoration Techniques, *QIRT 94, Eurotherm Series 42,* D. Balageas, G. Busse, and G.M. Carlomagno, Ed., EETI Editions, Paris, 1995
8. P.G. Bison, C. Bressan, R. Di Sarno, E. Grinzato, S. Marinetti, and G. Manduchi, Thermal NDE of Delaminations in Plastic Materials by Neural Network Processing, *QIRT 94, Eurotherm Series 42,* D. Balageas, G. Busse, and G.M. Carlomagno, Ed., EETI Editions, Paris, 1995
9. T.T.N. Lan, K. Haupt, U. Seidel, and H.G. Walther, Reconstruction of Thermal Defects from Photothermal Images, *QIRT 94, Eurotherm Series 42,* D. Balageas, G. Busse, and G.M. Carlomagno, Ed., EETI Editions, Paris, 1995
10. *Non-Destructive Evaluation and Quality Control*, Vol 17, *Metals Handbook*, 9th ed., ASM International, 1989